2021

CFD Analysis of an ORC Vane Expander using OpenFOAM Solver

Sham Ramchandra Rane
University of London, sham.rane@city.ac.uk

Giuseppe Bianchi
Brunel University London

Ahmed Kovačević
University of London

Roberto Cipollone
University of L'Aquila

CFD Analysis of an ORC Vane Expander using OpenFOAM solver

Sham RANE[1]*, Giuseppe BIANCHI[2], Ahmed KOVAČEVIĆ[1], Roberto CIPOLLONE[3]

[1]City, University of London, Centre for Compressor Technology,
London, EC1V 0HB, UK
sham.rane@city.ac.uk

[2]Brunel University London,
Uxbridge, UB8 3PH, UK
Giuseppe.Bianchi@brunel.ac.uk

[3]University of L'Aquila, Industrial and Information Engineering and Economics Department
L'Aquila 67100, Italy
roberto.cipollone@univaq.it

* Corresponding Author

ABSTRACT

Recent studies on the use of 3D Computational Fluid Dynamics (CFD) for the analysis and design of sliding vane machines has proved beneficial for the detailed evaluation and optimisation of the vane expanders for a given working fluid and operating condition. The authors have earlier developed a customised rotor grid generator for integration with commercial CFD solvers and validated it for use in typical small-scale ORC expanders for waste heat recovery. In this paper, this customised grid generation is extended to an open source CFD solver OpenFOAM, by using a connectivity methodology originally developed for roots blower and twin-screw machines. The control of the rotor grid deformation is through a user code integrated within the flow solver. A case study of the reference ORC expander operating with R245fa was used for validation. The available experimental data for three operating conditions are compared with the results calculated with ANSYS CFX and OpenFOAM-v1912 solvers. During the filling and expansion process, the internal pressure traces are accurately captured by both the solvers and the difference is within 0.05 bar with measurements. However, between the outlet port closure and inlet port opening process the pressure and temperature prediction with OpenFOAM solver is considerably different from the ANSYS CFX solver. It was observed that the OpenFOAM solver is resulting into a non-physical low temperature zone upstream to the tangency region of the rotor and the stator that goes below 80°C. Overall, CFD solution obtained with the commercial solver ANSYS CFX is much more stable and robust than the open source OpenFOAM solver. The generic nature of the deforming grid generation used with an open source CFD solver presented in the paper allows broadening of the utilisation of CFD modelling tools for the design of vane machines.

1. INTRODUCTION

Organic Rankine Cycle (ORC) expanders for heat to power generation use sliding vane machines. Off-design conditions are well accepted in terms of inlet thermodynamic properties of the working fluid, revolution speed, working fluid flow rates. These expanders show wider margins of flexibility when compared with the other machines and such advantages make them suitable for small size ORC-based power units to recover low-medium grade heat usually wasted into mechanical energy. However, the efficiency of rotary vane expanders may be lower than other positive displacement machines (Vodicka *et al.*, 2017). This is due to high volumetric losses, particularly the ones due to leakages between adjacent vanes which take place between the blade tip and the stator inner surface. A further limiting aspect of this machine is the fixed expansion ratio. In Yan *et al.* (2019), a variable expansion ratio rotary vane expander, which adjusts its expansion ratio by acting on the outlet opening angle has been investigated. To overcome some of these drawbacks, the concept of supercharging a vane expander was proposed. Supercharging the expander requires another suction port along the closed-volume expansion phase through which an additional quantity of

working fluid is supplied at the same suction conditions. In Fatigati *et al.* (2018a), using a 1-D thermo-fluid-dynamic model, validated on experiments performed using a single intake expander, an optimization analysis to define the circumferential position of the auxiliary port and its area which maximize the mechanical power produced was carried out. The results showed for the optimum configuration a 50% increase of mechanical power produced with respect the baseline case. In Fatigati *et al.* (2018b), an experimental comparison between single and dual intake expander was carried out keeping constant the intake and exhaust pressure. The results showed that the dual intake port expander can elaborate a 40% more of mass flow rate with an increase of indicated power of 50% in comparison of the original device. Nevertheless, the dual intake port expander allows to also improve the efficiency of the machine with respect to the baseline expander under certain condition and circumferential position of the auxiliary intake port. In fact, in Fatigati *et al.* (2019), an analytic relation which expresses the global efficiency difference between single and dual intake expander, keeping constant the intake and exhaust pressure, was found. Through this relation it was theoretically demonstrated if the increase of mass flow rate aspirated by the dual intake expander with respect the baseline case is lower than that of the mechanical power produced, the efficiency of the dual intake machine is higher. Fatigati *et al.* (2020), present a theoretical and experimental evaluation of a 2.0 kW vane expander and details of leakages inside the machine to quantify their effects on the expander performance. In order to achieve a deeper understanding of the supercharging process and its impact on the vane expander operation, Bianchi *et al.* (2019), performed numerical 3D CFD simulations using ANSYS CFX solver and SCORG grid generator on the machine developed and tested in earlier works. When operating at 1516 rpm and between pressures of 544 kPa at the inlet and 320 kPa at the outlet, the supercharged expander provided a power output of 325 W. The specific power output was equal to 3.25 kW/(kg/s) with a mechanical efficiency of 63.1%. For the CFD modelling strategy the essential requirement for the CFD modelling of a vane machine is the application of deforming working chamber grid and in Rane and Kovačević (2017a, 2017b), the grid generation using algebraic techniques has been extended to differential techniques in order to improve the mesh quality. The application in this study was with twin-screw compressors. This differential technique has been applied in Bianchi *et al.*, (2019) on the basic algebraic grid described in (Bianchi *et al.*, 2017a) and applied on the ORC expander analysis. The grid generation has been implemented in the customized grid generation tool SCORG (Kovačević *et al.*, 2005, 2007). The methodology developed in (Bianchi *et al.*, 2017b) was adopted to model the supercharged expander in (Bianchi *et al.*, 2019). The results show not only the successful model validation but also an extensive comparison between standard and supercharged machine. However, state-of-the-art research has been only applied to commercial CFD solvers. Initial works on application of open source CFD tools for analysis of positive displacement machines can be instead found in Casari *et al.* (2017). They presented a review of the techniques available with OpenFOAM-v1606+ solver. The application tested was a single screw expander. Casari *et al.* (2018a, 2018b, 2019) further developed an OpenFOAM interface with the customised grid generator SCORG and the application was demonstrated on Roots Blower and Twin-Screw Compressor with OpenFOAM-v1606+ solver. An oil injection study using lagrangian particle model in the Roots Blower application was presented in Casari *et al.* (2019) using with OpenFOAM-v1606+ solver and SCORG deforming grids for the rotor domains.

The objective of the presented analysis was to extend the use of customised grid generation with open source CFD solver OpenFOAM-v1912, by using a connectivity methodology originally developed for roots blower and twin-screw type of machines (Casari *et al.*, 2018a, 2018b, 2019). The rotor grid deformation was controlled through user code which works integrally with the flow solver. A case study has been presented on the reference ORC expander operating with R245fa (Bianchi *et al.*, 2019). Three operating conditions have been evaluated, for which experimental performance data are available for validation of the numerical methodology using ANSYS CFX and OpenFOAM-v1912 solvers. Through the analysis it was found that further research into the development of a robust and stable solver with positive displacement applications is required to account for the large grid deformation and volumetric changes that occur in these machines.

2. NUMERICAL ANALYSIS METHODOLOGY

Analysis of the ORC vane expander using OpenFOAM was carried out based on the available test data in literature and a corresponding, well established model in ANSYS CFX solver. Comparison with a validated ANSYS CFX model allowed for comparison of the detailed physics inside the expander for which numerical issues of the solver could be studied, together with their impact on prediction of the flow field.

2.1 ORC vane expander and test data

The supercharged expander was tested in an automotive ORC loop at the University of L'Aquila operating with R245fa. The expander is directly coupled with an asynchronous electric generator which constraints the expander to

rotate at slightly higher than 1500 RPM when the machine is connected to the electric grid. Further details on the test rig can be found in (Fatigati *et al.*, 2019). From an instrumentation perspective, two Coriolis mass flow meters are installed downstream the pump and on the primary inlet of the expander. Pressure and temperature transducers are located across each component of the ORC loop. The expander performance is eventually measured through a torque meter and through a set of 3 piezo-resistive pressure transducers. The overall expander dimensions are summarized in Table 1. The dual intake phase starts immediately after the end of the main one. Three test cases were selected to enable the CFD validation. A summary is reported in Table 2. Depending on the opening of the ball valve upstream of the secondary inlet, different supercharging ratios were achieved.

Table 1: Specification of the expander geometry

Number of Chambers	7
Stator Inner Diameter	75.90 mm
Rotor Outer Diameter	65.00 mm
Eccentricity	5.45 mm
Chamber Width	60.00 mm
Blade length	17.00 mm
Blade thickness	3.96 mm
Intake port opening angle	4.4 °
Intake port closing angle	48°
Exhaust port opening angle	180°
Exhaust port closing angle	320°
Tip clearance	25 µm

Table 2: Experimental data at three operating conditions of the expander

	Test case #1			**Test case #2**			**Test case #3**		
	p	T	m	p	T	m	p	T	m
	±0.3 bar_a	±0.3 °C	kg/s	±0.3 bar_a	±0.3 °C	kg/s	±0.3 bar_a	±0.3 °C	kg/s
Main Inlet (m ±0.15%)	4.55	66.1	0.047	5.44	94.3	0.061	5.57	82.3	0.055
Superchar. Inlet 2 **(m ±0.05%)**	4.75	66.1	0.054	4.74	94.3	0.039	5.77	82.3	0.064
Outlet	3.10	58.6		3.21	85.9		3.60	73.5	
Rev. speed (**±1 RPM**)	1511			1516			1517		
Torque (**±0.02 Nm**)	1.50			2.05			2.11		

The operating point that will be selected to show the validation of the CFD results is the test case #2, even though in (Bianchi *et al.*, 2019) the validation has been successful in all the operating points. At this point, there is limited supercharging which in turn leads to a 1bar pressure difference between the suction conditions of the primary line and the ones related to the supercharging port.

2.2 CFD Model description and OpenFOAM solver implementation

Rane and Kovačević (2017a) have presented the setup requirements for SCORG grid generator with widely used commercial CFD solvers. In case of vane expanders, Bianchi *et al.* (2019) presented the CFD model with supercharger using ANSYS CFX solver and the same has been employed in the current work. The working domain is split into five main sub-domains namely rotor domain, inlet port, supercharged inlet port, outlet port and axial end leakages as highlighted in Figure 1a. A sample cross-section of rotor grid is shown in Figure 1b.

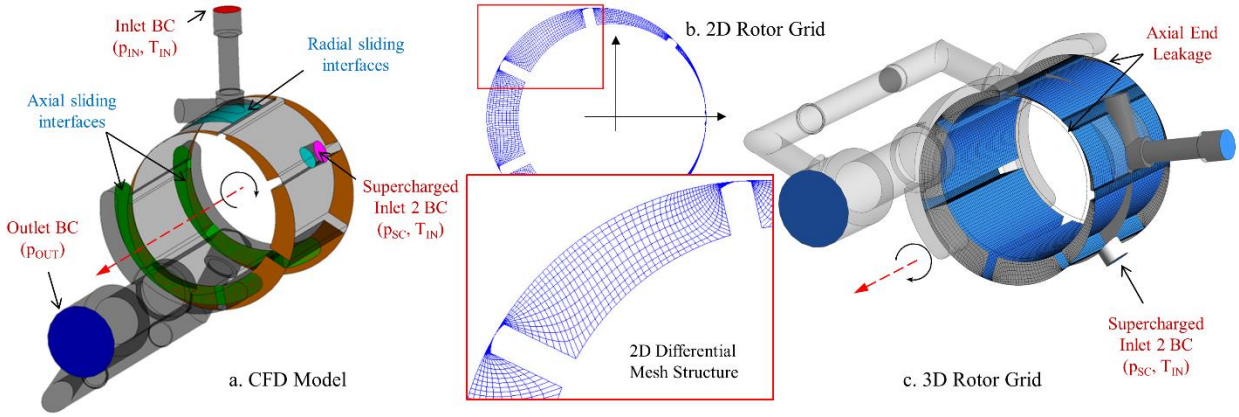

Figure 1: ORC vane expander, a) CFD Model showing various domains and boundaries, b) Grid in 2D cross-section and c) Grid of the rotor in 3D with alignment of ports and axial leakage

All sub-domains are connected within the solver using non-conformal interfaces as shown in Figure 1c. Supercharged inlet pressure was 4.74 bara with 94.3 °C gas temperature. Outlet pressure was 3.21 bara. The ideal gas model was used as the equation of state since it was found that the Peng-Robinson Real gas model was unstable in OpenFOAM-

v1912 solver, although it is recommended to use a real gas model in these operating conditions (Rane *et al.*, 2021). Dynamic viscosity, thermal conductivity and specific heat properties of the fluid R245fa are set constant. Table 3 and Table 4 provide the details of the specifications of the CFD solvers ANSYS CFX and OpenFOAM-v1912 respectively.

Table 3: Specification of the numerical setup in the ANSYS CFX solver

Mesh deformation	User defined nodal displacement	Advection scheme	High Resolution
Mesh in ports	Tetrahedral with boundary layer refinements (ANSYS Mesh)	Transient scheme	Second order Backward Euler
Turbulence model	SST – k Omega (Standard Wall Functions)	Transient inner loop coefficients	Up to 20 iterations per time step
Inlet/Supercharge boundary condition	Opening (Specified total pressure and temperature)	Convergence criteria	r.m.s residual level $1e^{-03}$
Outlet boundary condition	Opening (Static pressure, backflow acts as total pressure and temperature)	Relaxation parameters	Solver relaxation fluids (0.4)

Table 4: Specification of the numerical setup in the OpenFOAM-v1912 solver

Mesh deformation	SCORG – OpenFOAM Module	Advection scheme	First order - Upwind
Mesh in ports	Polyhedral (*SnappyHexMesh*)	Transient scheme	First order Backward Euler
Turbulence model	SST – k Omega (Standard Wall Functions)	Transient inner loop coefficients	Up to 20 iterations per time step
Inlet/Supercharge boundary condition	Opening (Specified total pressure and temperature)	Convergence criteria	r.m.s residual level $1e^{-03}$
Outlet boundary condition	Opening (Static pressure backflow acts as total pressure and temperature)	Relaxation parameters	Solver relaxation pressure (0.8), velocity (0.4), energy (0.8)

One of the other differentiating factors between the two solvers is the tetrahedral grid in ANSYS CFX and polyhedral grid generated by *SnappyHexMesh* utility in OpenFOAM, as represented for the inlet port in Figure 2a and Figure 2b respectively. The number of nodes and cells in the respective solvers is also listed in Figure 2.

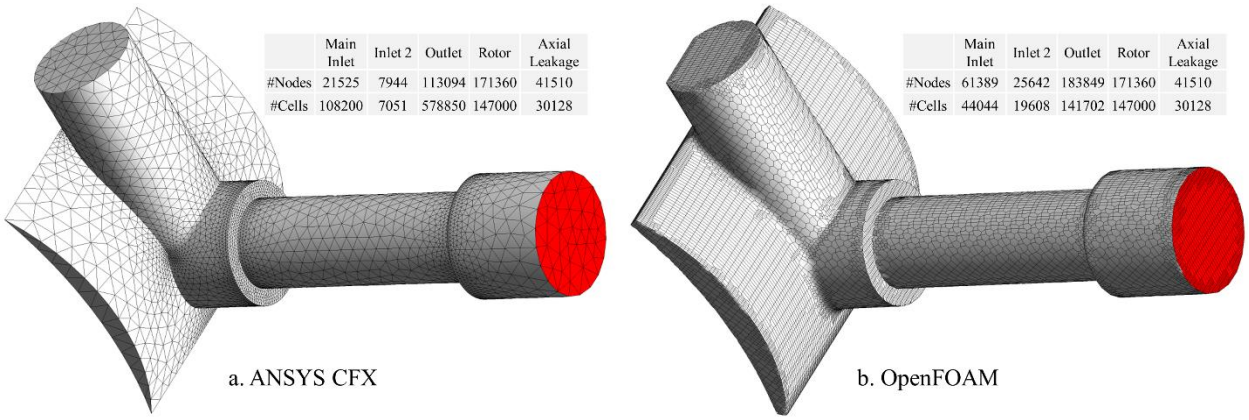

Figure 2: Grid structure in the port domain, a) ANSYS CFX – Tetrahedral, b) OpenFOAM – Polyhedral

Similarly, the supercharger port and the outlet port were both generated by *SnappyHexMesh* for OpenFOAM. The axial leakage grid was generated in ANSYS Meshing and used directly in ANSYS CFX solver. For OpenFOAM they were first converted using *fluentMeshToFoam* utility and then combined in the OpenFOAM setup. Thus, the rotor, tip and axial leakage grids are identical in both the solvers. ANSYS CFX utilized a vertex centered, pressure based coupled solution algorithm and total energy formulation. Whereas OpenFOAM solver was cell centered, set with the compressible *rhoPimpleFoam* segregated solver with *sensibleEnthalpy* energy formulation.

ANSYS CFX provides a coupling feature called Junction Box Routine that is a user defined library to specify mesh deformation from custom applications such as SCORG. The solver updates the nodes coordinates from set of pre-generated coordinate files after every crank angle step (or its submultiples). Solver time step size finally results from the selected crank angle step (at which the customized grids are generated) and revolution speed of the rotor. In this

case study, the full rotation of the rotor was defined by 700 grid positions. In case of OpenFOAM, a customised SCORG module was developed (Casari *et al.*, 2018a, 2018b, 2019). Table 5 provides the implementations details of this SCORG – OpenFOAM interface in terms of the parameters of the two dictionaries that control mesh deformation in the solver based on the set of rotor grids supplied from SCORG grid generator. Solver is allowed to use time step interpolation in this interface in order to set an independent time step size, but for consistency with ANSYS CFX solver, the time interpolation of grid was not used in these case studies.

Table 5: Implementation parameters of SCORG – OpenFOAM interface

Dictionary	Parameter	Value	Usage
SCORGDict	conformalInterface	True/False	Distribution selected in SCORG is Rotor-to-Casing **Conformal** set this as True
	nonConformalInterface	True/False	Distribution selected in SCORG is Rotor-to-Casing **Non-Conformal** set this as True
	rotorToCasing	True/False	Distribution selected in SCORG is Rotor-to-Casing set this as True, otherwise set as False
	singleRotor	True/False	Calculations involving only one rotor. Vane Compressor, Set as True, Else Set as False
	lowPressurePort	True/False	Theoretical **Suction Port** from SCORG transferred to OpenFOAM, Set as True
	highPressurePort	True/False	Theoretical **Discharge Port** from SCORG transferred to OpenFOAM, Set as True
	prisms	True/False	Convert the hexahedral cells into prisms using this tag
dynamicMeshDict	frozenPointsZone	frozenPointsZone	Collector for port nodes - do not apply mesh deformation
	malePointsZone	malePointsZone	Collector for main rotor nodes - Apply mesh deformation
	femalePointsZone	femalePointsZone	Collector for gate rog nodes - Apply mesh deformation
	conformal	True/False	Set True in case of Type of Distribution selected in SCORG is Rotor-to-Casing Conformal
	numberOfGrids	700	Number of Grid files written from SCORG for one cycle
	numberOfGrooves	1	Number of Lobes on the Main Rotor. In case of Vane rotor = 1
	omega	1511	Rotor speed in revolutions per minute units

Initial conditions for the flow solver were provided as constant pressure and temperature values and the calculations were performed for 1400 time steps in every case which represent 14 expansion cycles (2 full machine revolutions). The rotor speed, inlet and outlet pressure and temperature listed in Table 2 are used as boundary condition specifications for the CFD model. The results were found to converge in the first few cycles for pressure and torque but took a little longer for outlet temperature. Data from the last few converged cycles has been used here for results presentation in the next section.

3. RESULTS AND DISCUSSION

The analysis results are presented here as comparison of operating condition of Test case #2 for each of the two solvers ANSYS CFX and OpenFOAM-v1912. Two variants of the CFD model were investigated, identified as Case A and Case B respectively for each of the three operating conditions. Case A has 25 µm tip leakage clearance and Case B additionally has two axial leakage clearances of 50 µm introduced at both the rotor ends as indicated in Figure 1c.

3.1 Internal pressure and temperature distribution

A comparison of internal pressure distribution during the filling, expansion and supercharging process followed by further expansion is presented in Figure 3 between the measured data and Case 2-A and Case 2-B with ANSYS CFX solvers.

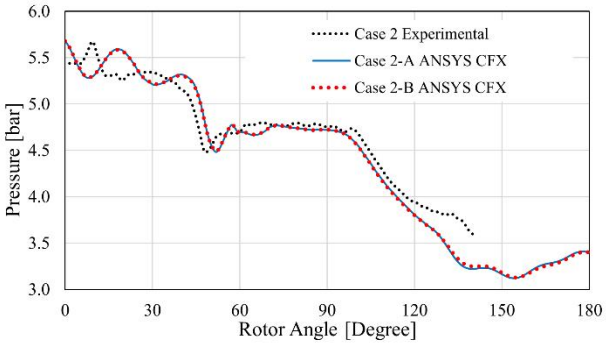

Figure 3: Comparison of pressure with vane rotation angle during filling and expansion process

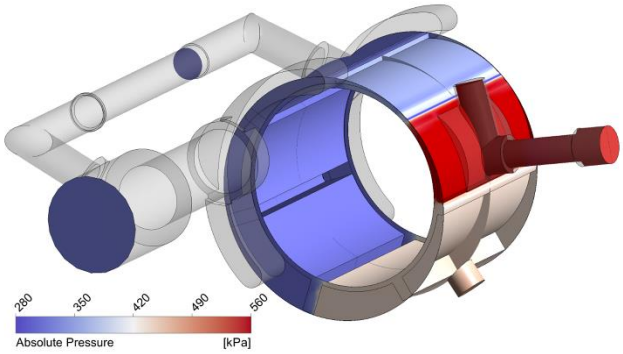

Figure 4: Instantaneous pressure distribution in the vane rotor and ports for Case 2-B ANSYS CFX

It can be seen in these stages of the expander; the internal pressure traces are accurately captured and between 30-100° rotor angle the difference is within 0.05 bar with measurements. The introduction of 50 µm end leakage in Case 2-B did not produce a significant influence on the internal pressure trace as it closely matches the Case 2-A data. The initial flow pulsations, dip in pressure at around 55° rotor angle, followed by a re-filling from the supercharged inlet is captured by the internal pressure traces. In correspondence to these data, an instantaneous distribution of pressure in the expander is shown in Figure 4 for Case 2-B with the ANSYS CFX solver. The peak pressure in the chamber at this rotor position, where one of the vane is at tangency to the stator, is 560 kPa. While the lowest pressure is seen to be close to 280 kPa which occurs at the tangency vane's tip region where flow velocity is high.

A cross-section of the expander at mid-length of the rotor is evaluated in Figure 5. Figure 5a is a contour plot for Case 2-A and ANSYS CFX solver, while Figure 5b is a corresponding plot of pressure for Case 2-A and OpenFOAM solver. Five monitor probes are located in this cross-section identified as Probe-1 to Probe-5. Data at these probes will be compared between the two solvers. On examination of Figure 5, a closeness of the pressure results between the two solvers is evident. Angular positions of significance such as closure of the main and supercharged inlet and opening of the outlet have been marked in Figure 5. As observed with ANSYS CFX solver in Figure 4, the peak pressure in the chamber at this rotor position is 560 kPa and the lowest pressure is close to 280 kPa in the OpenFOAM solver too.

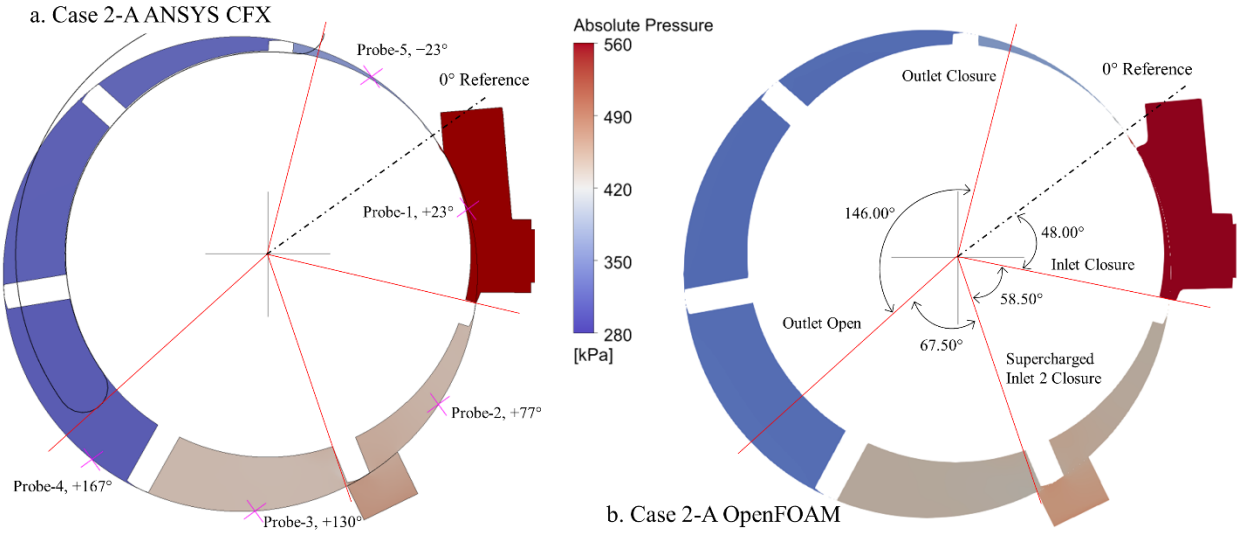

Figure 5: Monitor probe locations and pressure distribution in the expander cross-section at z=0.03 m, a) Case 2-A ANSYS CFX, b) Case 2-A OpenFOAM

Probe locations Probe-1 to Probe-4 are evaluated in the plots of Figure 6 where pressure and temperature data over one full cycle of the vanes has been compared for Case 2-A, between the two solvers. Probe-1 is overlapped on the main inlet. Hence the pressure at the location remains very close to the range of 520 – 560 kPa. Flow pulsations cause the pressure to vary from the condition of 544 kPa at the main inlet. Probe-1 is not exposed to the supercharged inlet. Probe-2 is located such that at 25° rotor angle it gets exposed to the supercharged inlet. Hence in the 0-25° range the initial expansion has caused the chamber pressure to drop to about 450 kPa and it fills back to 540 kPa supercharged inlet pressure at 25°. Probe-3 starts with a chamber pressure of 450 kPa which steadily drops to 350 kPa as expansion is progressing and at 25° rotor angle the probe gets exposed to the chamber which is open to supercharged inlet port. This results in a rise in probe pressure to 460 kPa over the remaining cycle duration. Probe-4 is located open to the outlet port from 0-10° rotor angle. Following which it gets into the expansion chamber at 390 kPa and steady drop in pressure is observed in the remaining cycle. A systematic variation of pressure in the chamber is observed from the Figure 6a plots. The results between ANSYS CFX and OpenFOAM solvers are comparable and the local differences are of the order of 10-15 kPa over the cycle.

A comparison of temperature data (Figure 6b) at these probes also follows a similar trend. But since gas temperature has significantly higher local variation, the point probes are not able to represent the chamber's average property. Nevertheless, probe data from ANSYS CFX solver and OpenFOAM solvers is close to each other over most of the cycle span. Large differences are seen at each of the Probe-1 - Probe-4 when the transition of the vane happens. At these rotor angles the points are exposed to the tip leakage gas and data generated by the two solvers is different in

these regions, thus indicating a difference is accuracy of the solver in these critical regions. Typically, OpenFOAM solver is producing a dip in the gas temperature when the vane tip approaches the probe location, while the ANSYS CFX solver is producing a jump. This can be observed at Probe-2 and Probe-3 in 20-25° rotor angle and Probe-4 in 5-12° rotor angle. Probe-1 with ANSYS CFX solver is uniform as it is exposed to the inlet port, but with OpenFOAM solver there is non-physical jump at 30° rotor angle from 94°C inlet temperature to about 98°C.

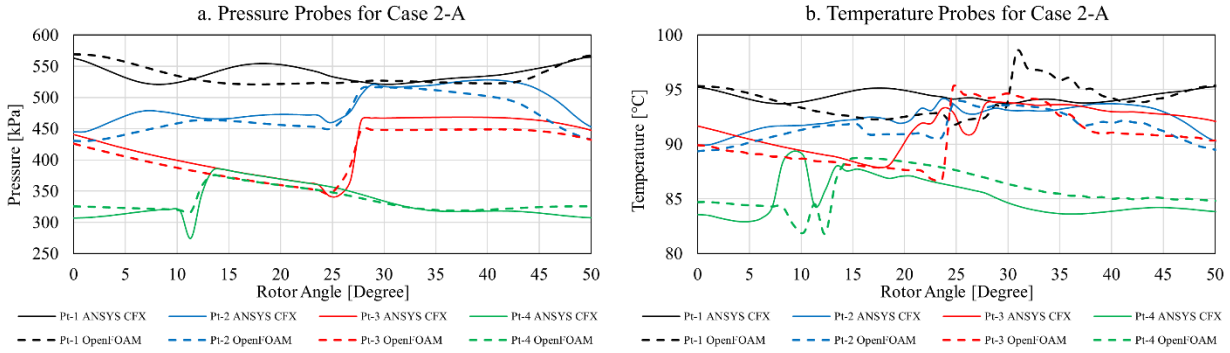

Figure 6: Comparison of pressure (a) and temperature (b) data at Probe-1, 2,3 and 4 locations for Case 2-A

The location of Probe-5 is distinct and not in the expansion cycle. It is located between the outlet port closure and inlet port opening rotor angle range as indicated in Figure 5. The pressure and temperature data over one full cycle of the vanes has been compared for Case 2-A and Case 2-B between the two solvers in Figure 7. After about 5° rotor angle the chamber containing Probe-5 disconnects from the outlet port and pressure starts to rapidly increases. In Case 2-A ANSYS CFX solver the peak pressure reaches close to about 700 kPa. In Case 2-B ANSYS CFX solver, the presence of axial leakage flow reduces this peak pressure to about 650 kPa. After 18° rotor angle the pressure starts to drop at Probe-5 and at the vane transition at 27° the least pressure of 210 kPa is observed in both Case 2-A and Case 2-B. Following this, the pressure in the chamber remains uniform at about 350 kPa till the end of the cycle. The pressure prediction with OpenFOAM solver is considerably different from the ANSYS CFX solver at Probe-5 in both Case 2-A and Case 2-B. As seen in Figure 7, the peak pressure with OpenFOAM solver is nearly 1100 kPa with Case 2-A and close to 1000 kPa with Case 2-B. Since the experimental data of internal pressure is not available at this probe location, it is difficult to validate the results in Figure 7. The temperature data plots in Figure 7 indicate a similar trend in results. Peak temperature in ANSYS CFX solver reaches close to 117°C in Case 2-A and 115°C in Case 2-B. Whereas with OpenFOAM solver the peak temperature is close to 122°C in both Case 2-A and Case 2-B. An odd effect is seen in the OpenFOAM solver that gas temperature in the 0-25° rotor angle is higher in Case-2B, which in the presence of axial leakage is expected to be lower than in Case 2-A.

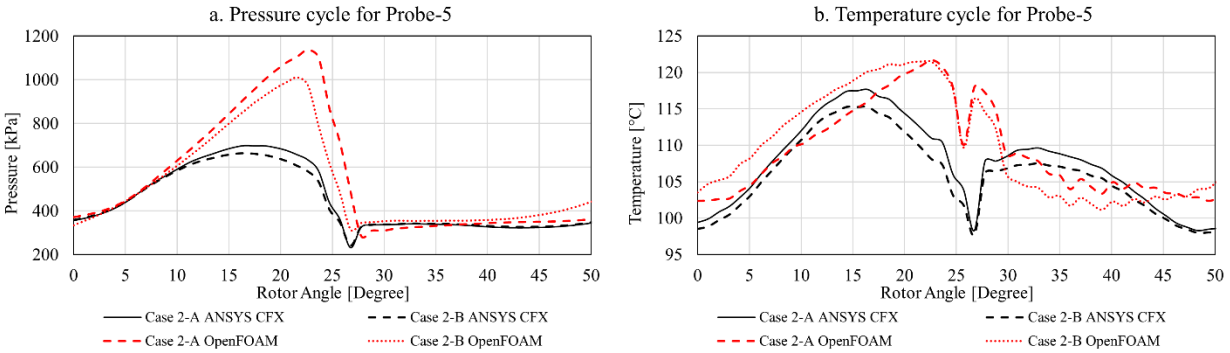

Figure 7: Comparison of pressure (a) and temperature (b) cycle data at Probe-5 location

To test these results further, the temperature distribution in the expander domain is compared between Case 2-B ANSYS CFX and Case 2-B OpenFOAM solvers in Figure 8. Figure 8a with ANSYS CFX solver indicates a uniform distribution of temperature upstream of the tangency region and a local dip at the tip of the vane to about 85°C. In Figure 8b it is seen that the OpenFOAM solver is resulting into a non-physical low temperature zone upstream to the tangency region of the rotor and the stator that goes below 80°C. Probe-5 data in Figure 7 does not capture this local

low temperature zone, but it was found to be close to 65°C from data. Within the same chamber the adjacent gas temperature exceeds 105°C and this odd nature of the results can be attributed to numerical inaccuracies.

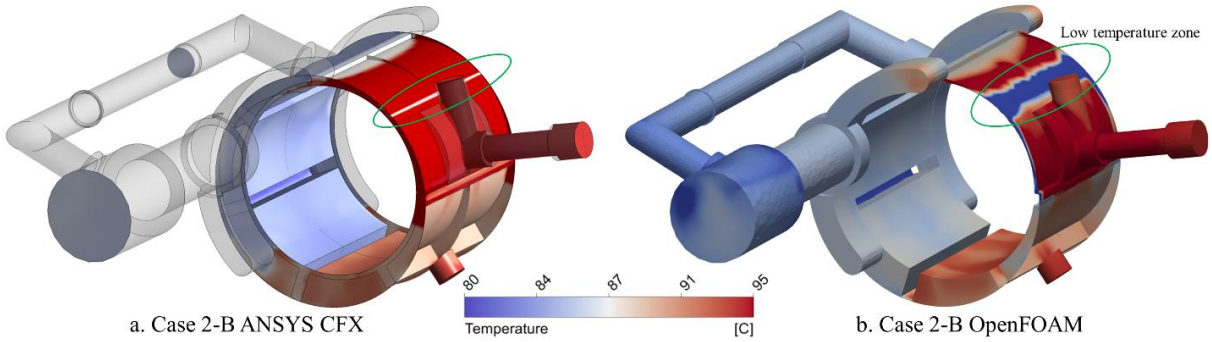

Figure 8: Comparison of instantaneous temperature distribution in the vane rotor and ports, a) Case 2-B ANSYS CFX, b) Case 2-B OpenFOAM

3.2 Comparison of mass flow rate and rotor torque cycles

A cyclic variation of the gas mass flow rate at main inlet and supercharged inlet is presented over three consecutive cycles in Figure 9. Cases 2-A with both the ANSYS CFX and OpenFOAM solver have been plotted here for comparison. The corresponding cycle averaged mass flow rates are reported in Table 6. A clear repetition of the flow is apparent from Figure 9 indicating that the solution is being well converged. Case 2-A main and supercharged inlet have different nature of variation. Main inlet being further from the rotor shows smoother variation with two pulses per cycle. Relatively, OpenFOAM Case 2-A main and supercharged inlet have a different nature of flow variation. This could be due to the difference in implementation of the total pressure boundary condition in the two flow solvers.

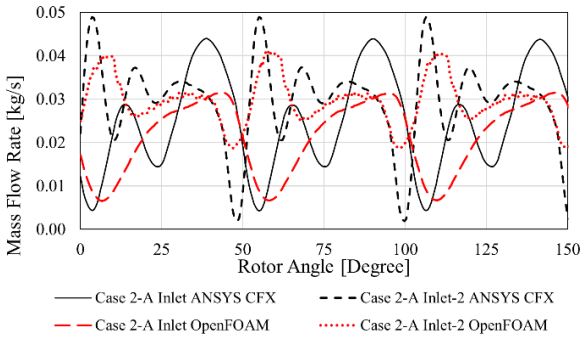

Figure 9: Comparison of cyclic mass flow rate at the two inlets (3 cycles)

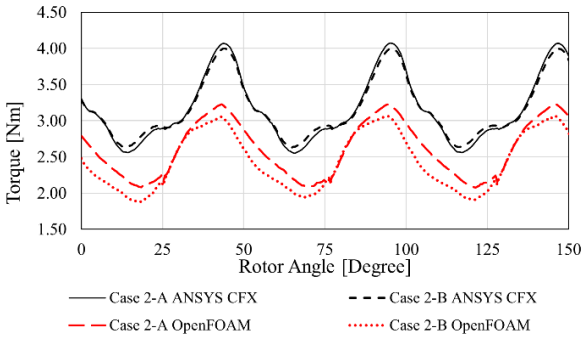

Figure 10: Comparison of cyclic torque on the vane rotor (3 cycles)

Similarly, a cyclic variation of the rotor torque over three consecutive cycles is presented in Figure 10 for Case 2-A and Case 2-B with both the solvers. Cycle averaged rotor torque is reported in Table 6. Unlike the flow variation, the nature of torque variation is similar in both the solvers. But it is clear from the plot that average torque in OpenFOAM solver is lower as compared to ANSYS CFX solver for both Case 2-A and Case 2-B. The difference between Case 2-A and Case 2-B is minor in ANSYS CFX as compared to OpenFOAM indicating a stronger influence of the axial leakage flow. The drop in peak pressure from 1100 kPa to 1000 kPa at Probe-5 indicated in Figure 7 is required to be noted here which could impact the rotor torque significantly.

3.3 Comparison of the expander performance

Performance data of the expander is obtained from the CFD model in terms of cyclically averaged mass flow rate at the main and supercharged inlets, gas temperature at the outlet, torque on the vane rotor and expander power at corresponding rotor speed. These performance data from ANSYS CFX and OpenFOAM solvers has been compared with test data available in Table 2 and the comparison has been presented here in Table 6. Expander specific power is obtained from the net mass flow rate of R245fa from both inlets and the power.

Table 6: Comparison of expander integral performance quantities

25 µm Tip, 0 µm Axial clearance	**Case 1 - A**			**Case 2 - A**			**Case 3 - A**		
Parameter	Measurement	ANSYS CFX	OpenFOAM	Measurement	ANSYS CFX	OpenFOAM	Measurement	ANSYS CFX	OpenFOAM
Inlet mfr [kg/s]	0.0470	0.0203 56.71%	0.0185 60.61%	0.0610	0.0251 58.92%	0.0215 64.75%	0.0550	0.0242 56.07%	0.0219 60.18%
SC inlet mfr [kg/s]	0.0540	0.0370 31.39%	0.0353 34.63%	0.0390	0.0290 25.66%	0.0294 24.73%	0.0640	0.0430 32.76%	0.0411 35.79%
Outlet T [°C]	58.60	58.93 -0.57%	60.60 -3.41%	85.90	85.50 0.47%	86.00 -0.12%	73.50	73.86 -0.49%	74.00 -0.68%
Torque [Nm]	1.50	2.76 -83.93%	2.13 -41.72%	2.05	3.17 -54.73%	2.61 -27.51%	2.11	3.78 -79.21%	3.05 -44.69%
25 µm Tip, 50 µm Axial clearances	**Case 1 - B**			**Case 2 - B**			**Case 3 - B**		
Parameter	Measurement	ANSYS CFX	OpenFOAM	Measurement	ANSYS CFX	OpenFOAM	Measurement	ANSYS CFX	OpenFOAM
Inlet mfr [kg/s]	0.0470	0.0204 56.67%	0.0180 61.71%	0.0610	0.0257 57.83%	0.0214 64.93%	0.0550	0.0242 55.93%	0.0214 61.12%
SC inlet mfr [kg/s]	0.0540	0.0381 29.43%	0.0360 33.39%	0.0390	0.0295 24.40%	0.0299 23.27%	0.0640	0.0443 30.79%	0.0420 34.42%
Outlet T [°C]	58.60	59.12 -0.88%	60.00 -2.39%	85.90	86.00 -0.12%	86.00 -0.12%	73.50	74.29 -1.07%	75.00 -2.04%
Torque [Nm]	1.50	2.76 -83.89%	1.96 -30.86%	2.05	3.17 -54.72%	2.45 -19.43%	2.11	3.78 -79.26%	2.88 -36.72%

In Cases A when there is no axial end leakage, the mass flow rate through the main and the supercharged inlet is consistently lower than Cases B at all the three operating conditions. This is estimated by both ANSYS CFX and OpenFOAM solvers. Within each operating condition, OpenFOAM solver is underestimating both the main inlet and supercharged inlet mass flow rate as compared to ANSYS CFX solver. Since a number of leakage paths were discarded, e.g. the clearance gaps between rotor slots and each of the seven blades, both solvers are underpredicting mass flow rate in comparison to the measurements. The difference is significantly larger for the main inlet flow. Outlet gas temperature is sufficiently accurately predicted by the CFD models as compared to the measurements. Overall, OpenFOAM is resulting into 0.5-1.5°C over estimation of the outlet temperature in all cases. This is an odd result considering that the total mass flow rate is relatively lower in the OpenFOAM cases and hence after expansion the gas temperature drop is expected to be higher. This is likely due to the simplified real gas model adopted. The rotor torque is overestimated by both ANSYS CFX and OpenFOAM models as compared to measurements. Since the peak pressure observed at Probe-5 is much higher in OpenFOAM results, this creates an opposing rotor torque. Thus relatively, OpenFOAM torque results are closer to measurements even though internal pressure variation during expansion is similar in both the solvers. Due to a lower total mass flow rate, the specific power calculated from OpenFOAM is lower than ANSYS CFX across all the cases but in both the solvers it is highly overestimated as compared to measurements. This is due to significantly higher rotor torque.

4. CONCLUSIONS

The analytical and differential grid generation methods built in the software SCORG are available for the rotating and deforming domain of vane machines and well-integrated with commercial CFD solvers. In the work presented in this paper, this customised grid generation has been extended to an open source CFD solver OpenFOAM, by using a connectivity methodology SCORG-OpenFOAM module, originally developed for roots blower and twin-screw machines. The rotor grid deformation was controlled through the user code integrated within the flow solver. A case study has been presented on a reference ORC expander operating with R245fa. Three operating conditions have been evaluated using ANSYS CFX and OpenFOAM-v1912 solvers and compared with the available experimental performance in order to validate this numerical methodology.

- The CFD solution obtained with the commercial solver ANSYS CFX is much more stable and robust than the open source OpenFOAM solver. Further, the real gas equation of state could not be used for R245fa fluid due to the instability of the OpenFOAM solver. In a separate exercise, ANSYS CFX solver obtained stable and converged results with all real gas models including REFPROP, Peng-Robinson and others.
- The indicated pressure traces obtained by the experiment and through simulation agreed well in both solvers during the filling and expansion processes. However, a large difference in the peak pressure and temperature was noticed in the process following the closure of the outlet port.

- A comparison of local temperature distribution indicated that the OpenFOAM solver is resulting into a non-physical, low temperature zone upstream to the tangency region of the rotor and the stator.
- Cycle averaged expander performance data was comparable between the two solvers. The mass flow rate through the main inlet was under predicted whiled the rotor torque was over predicted by the OpenFOAM solver.

The generic nature of the deforming grid generation together with an open source CFD solver is available to broaden the utilisation of CFD modelling tools for the design of vane machines. However, further research to improve robustness and stability of the solver for calculation of positive displacement machines is required, in order to account for the large grid deformation and large volumetric changes that occur in these machines.

REFERENCES

Bianchi, G., Rane, S., Kovačević, A. & Cipollone, R. (2017a). Deforming grid generation for numerical simulations of fluid dynamics in sliding vane rotary machines, *Advances in Engineering Software*, 112, 180-191, ISSN 0965-9978, DOI:10.1016/j.advengsoft.2017.05.010.

Bianchi, G., Rane, S., Kovačević, A., Cipollone, R., Murgia, S. & Contaldi, G. (2017b). Numerical CFD simulations on a small-scale ORC expander using a customized grid generation methodology, *Energy Procedia*, 129, 843-850, ISSN 1876-6102, DOI:10.1016/j.egypro.2017.09.199.

Bianchi, G., Rane, S., Fatigati, F., Cipollone, R. & Kovačević, A. (2019). Numerical CFD simulations and indicated pressure measurements on a sliding vane expander for heat to power conversion applications. *Designs*. 3(31). DOI: 10.3390/designs3030031.

Casari, N., Suman, A., Ziviani, D., van den Broek, M., De Paepe, M. & Pinelli, M. (2017). Computational Models for the Analysis of positive displacement machines: Real Gas and Dynamic Mesh, *Energy Procedia*, 129, 411-418, ISSN 1876-6102, DOI: 10.1016/j.egypro.2017.09.124

Casari, N., Fadiga, E., Pinelli, M., Suman, A., Kovačević, A., Rane, S. & Ziviani, D. (2018a). Full 3D numerical analysis of a roots blower with open-source software. 24th International Compressor Engineering Conference at Purdue. Paper 2620. https://docs.lib.purdue.edu/icec/2620

Casari, N., Pinelli, M., Suman, A., Kovačević, A., Rane, S. & Ziviani, D. (2018b). Full 3D numerical analysis of a twin screw compressor by employing open-source software. International Conference on Screw Machines. IOP Conf. Ser.: *Mater. Sci. Eng.,* 425, 012017. DOI: 10.1088/1757-899X/425/1/012017

Casari, N., Fadiga, E., Pinelli, M., Suman, A., Kovačević, A., Rane, S. & Ziviani, D. (2019). Numerical investigation of oil injection in a Roots blower operated as expander. International Conference on Compressors and their Systems. IOP Conf. Ser.: *Mater. Sci. Eng.*, 604, 012075. DOI: 10.1088/1757-899X/604/1/012075

Fatigati, F., Bianchi, G. & Cipollone, R. (2018a). Development and numerical modelling of a supercharging technique for positive displacement expanders, *Applied Thermal Engineering*, 140, 208-216, ISSN 1359-4311, DOI:10.1016/j.applthermaleng.2018.05.046.

Fatigati, F., Bartolomeo, M. D. & Cipollone, R. (2018b). Experimental and numerical characterization of a positive displacement vane expander with an auxiliary injection port for an ORC-based power unit, *Energy Procedia*, 148, 830-837, ISSN 1876-6102, DOI:10.1016/j.egypro.2018.08.114.

Fatigati, F., Bartolomeo, M. D. & Cipollone, R. (2019). Dual intake rotary vane expander technology: Experimental and theoretical assessment, *Energy Conversion and Management*, 186, 156-167, ISSN 0196-8904, DOI:10.1016/j.enconman.2019.02.026.

Fatigati, F., Bartolomeo, M. D. & Cipollone, R. (2020). On the effects of leakages in Sliding Rotary Vane Expanders, *Energy*, 192, 116721, ISSN 0360-5442, DOI: 10.1016/j.energy.2019.116721

Kovačević, A. (2005). Boundary Adaptation in Grid Generation for CFD Analysis of Screw Compressors, *Int. Num. Eng*., 64(3), 401-426.

Kovačević, A., Stošić, N. & Smith, I. K. (2007). *Screw compressors - Three dimensional computational fluid dynamics and solid fluid interaction*, ISBN 3-540-36302-5, Springer-Verlag Berlin Heidelberg New York.

Qiu, G., Liu, H. & Riffat, S. (2011). Expanders for micro-CHP systems with organic Rankine cycle, *Applied Thermal Engineering*, 31(16), Pages 3301-3307, ISSN 1359-4311. DOI:10.1016/j.applthermaleng.2011.06.008

Rane, S. & Kovačević, A. (2017a). Application of numerical grid generation for improved CFD analysis of multiphase screw machines, 10th International conference on compressors and their systems, London, IOP Conf. Ser.: *Mater. Sci. Eng.*, 232, 01. DOI:10.1088/1757-899X/232/1/012017

Rane, S. & Kovačević, A. (2017b). Algebraic generation of single domain computational grid for twin screw machines. Part I. Implementation, *Advances in Engineering Software*, 107, 38-50.

Rane, S., Kovačević, A., Stošić, N. & Smith, I. (2021). Analysis of real gas equation of state for CFD modelling of twin screw expanders with R245fa, R290, R1336mzz(Z) and R1233zd(E). *International Journal of Refrigeration*. 121:313-326. DOI: 10.1016/j.ijrefrig.2020.10.022.

Vodicka, V., Novotny, V., Mascuch, J. & Kolovratnik, M. (2017). Impact of major leakages on characteristics of a rotary vane expander for ORC, *Energy Procedia*, Volume 129, 387-394, ISSN 1876-6102, DOI:10.1016/j.egypro.2017.09.249.

Yan, J., Han, Y., Tian, J., Xu, Y., Zhang, Y. & Chen, R. (2019). Performance investigation of a novel expander coupling organic Rankine cycle: Variable expansion ratio rotary vane expander for variable working conditions, *Applied Thermal Engineering*, 152, 573-581, ISSN 1359-4311, DOI:10.1016/j.applthermaleng.2019.02.103.

ACKNOWLEDGEMENT

Authors would like to thank Professor M. Pinelli, Dr. N. Casari and Mr. E. Fadiga from University of Ferrara, Italy, for development of the SCORG-OpenFOAM interface and their help in setting the CFD test case.